

Teleoperation with Adaptive Motion/Force Control

Wen-Hong Zhu

S. E. Salcudean

Dept. of Electrical and Computer Engineering
University of British Columbia
2356 Main Mall, Vancouver, BC
Canada V6T 1Z4

Abstract

In this paper, an adaptive motion/force control based approach is proposed to control bilateral teleoperation systems under both position and rate control with arbitrary motion/force scaling. The master and the slave are treated separately, and are subject to independent adaptive motion/force control. A model of the human operator is incorporated into the dynamics of the master robot, while a model of the environment is incorporated into the dynamics of the slave robot. L_2 and L_∞ stability is guaranteed for both position/velocity tracking between the master/slave robots. The overall teleoperation system is equivalent to a free-floating mass plus a linear damper specified by the control and scaling parameters only. This approach possesses three features compared to previous teleoperation approaches: a) it is L_2 and L_∞ stability guaranteed with motion/force tracking capability, b) it can handle parameter uncertainties by applying independent parameter adaptation, and c) it takes into account the full nonlinear dynamics of the master/slave robots. The validity of the theoretical results are verified by experiments.

1 Introduction

Teleoperated control has been extensively studied, motivated by a large variety of applications [1], ranging from nuclear operations and space explorations to forestry-related tasks and medical applications. Teleoperation can extend a human's operation to a remote site or can enhance a person's capability to handle both the macro and the micro world. The goal of teleoperation is to let the slave track the motion of a human-controlled master and let the human operator have a precise perception with force feedback from the slave.

A typical teleoperation system consists of a master manipulator, a slave manipulator, the human operator, and the operated environment. Hannaford [2] proposed a two-port model based on circuit theory. Ideal trans-

fer functions are presented and the system deviation from the ideal response is suggested to be due to the inadequate cancellation of the mechanism impedances. Kosuge *et al.* [3] proposed an approach to control a single-master and multi-slave manipulator system by using a *virtual internal model*. This approach is based on the complete cancellation of robot dynamics. Anderson and Spong [4] addressed the time delay issue in maintaining stability for bilateral teleoperation. They used scattering operators to design a controller in such a way that stability is guaranteed with strictly passive operators and environments. Although asymptotic stability is ensured [5], no motion/force tracking is provided. Therefore, this scheme may result in poor transparency [6]. Lawrence [6] indicated the conflicting issues between stability and transparency and proposed a unified four-channel control structure. Perfect transparency with ideal kinesthetic feedback was achieved in [7] provided that the master/slave manipulators are with known dynamic parameters and with measurable accelerations. Colgate [8] proposed an impedance shaping control scheme to deal with different impedance and different geometric scales between the task and the human operator. Robustness criteria were discussed to ensure stability for passive operators and environments.

Unlike the schemes mentioned above, the novel teleoperation controller presented in this paper does not use the two-port model. Instead, the master robot and the slave robot are treated separately, and are subject to independent adaptive motion/force control. L_2 and L_∞ stability is guaranteed for motion tracking between the master/slave robots. The overall teleoperation system behaves as a free-floating mass plus a linear damper specified by the control and scaling parameters only. In Section 2, the adaptive control of each master/slave robot controller is presented. Section 3 proposes a bilateral teleoperation design method. A block diagram representation is given in Section 4. Section 5 demonstrates the experimental results. Finally, conclusions are drawn in Section 6.

where $\mathcal{V}_{\gamma d} \in R^6$ denotes a given command. $\mathcal{K} \in R^{6 \times 6}$ is a positive-definite feedback gain matrix. $A \in R^{6 \times 6}$ in (11) is a diagonal positive-definite matrix with small elements. $\tilde{\mathcal{F}}_{\gamma} \in R^6$ denotes a filtered force governed by

$$\dot{\tilde{\mathcal{F}}}_{\gamma} + C \cdot \tilde{\mathcal{F}}_{\gamma} = C \cdot \mathcal{F}_{\gamma} \quad (12)$$

where $C \in R^{6 \times 6}$ is a diagonal positive-definite matrix. $\hat{\mathcal{P}}$ denotes the estimate of parameters \mathcal{P} in the linear regression

$$\mathcal{Y} \cdot \mathcal{P} = \mathcal{M} \cdot \frac{d}{dt} [\mathcal{T} \cdot (\mathcal{V}_{\gamma d} - A \cdot \tilde{\mathcal{F}}_{\gamma})] + \mathcal{C} \cdot \mathcal{T} \cdot (\mathcal{V}_{\gamma d} - A \cdot \tilde{\mathcal{F}}_{\gamma}) + \mathcal{G} \quad (13)$$

The block diagonal property of \mathcal{M} and \mathcal{C} makes \mathcal{Y} block diagonal. The control law (11) requires measured velocity \mathcal{V}_{γ} and force \mathcal{F}_{γ} (see (12)).

In order to deal with parameter uncertainties, a decentralized parameter adaptation is proposed as

$$\begin{aligned} \dot{\hat{\mathcal{P}}}_i &= \rho_i \cdot \kappa_i \cdot s_i \\ s_i &= \mathcal{Y}_i^T \cdot \mathcal{T} \cdot (\mathcal{V}_{\gamma d} - \mathcal{V}_{\gamma} - A \cdot \tilde{\mathcal{F}}_{\gamma}) \\ \kappa_i &= \begin{cases} 0 & \hat{\mathcal{P}}_i \leq \mathcal{P}_i^- \text{ and } s_i \leq 0 \\ 0 & \hat{\mathcal{P}}_i \geq \mathcal{P}_i^+ \text{ and } s_i \geq 0 \\ 1 & \text{otherwise} \end{cases} \end{aligned} \quad (14)$$

where $\rho_i > 0$ is the update gain for the i th parameter \mathcal{P}_i . \mathcal{Y}_i denotes the i th column of \mathcal{Y} , and \mathcal{P}_i^- and \mathcal{P}_i^+ denote lower and upper bounds on \mathcal{P}_i . Because $\mathcal{P}_i \in [\mathcal{P}_i^-, \mathcal{P}_i^+]$, it follows from (14) that

$$(\mathcal{P}_i - \hat{\mathcal{P}}_i) \cdot (s_i - \dot{\hat{\mathcal{P}}}_i / \rho_i) \leq 0 \quad (15)$$

The parameter adaptation (14) can be performed with respect to each parameter independently. In view of $\dot{q}_j = \mathcal{Y}_{i(j)}^T \cdot \mathcal{T} \cdot \mathcal{V}_{\gamma}$, (11), and (14), the estimate of d_j defined in (7) obeys $\dot{d}_j = \rho_{i(j)} \int_0^t (\dot{q}_{jd} - \dot{q}_j) dt$, where $\rho_{i(j)}$ is a big positive constant. This is a strong integral of the joint velocity error and leads to zero steady-state velocity error.

A non-negative function is chosen as

$$\begin{aligned} V &= \frac{1}{2} \cdot (\mathcal{V}_{\gamma d} - \mathcal{V}_{\gamma} - A \cdot \tilde{\mathcal{F}}_{\gamma})^T \cdot \mathcal{T}^T \cdot \mathcal{M} \cdot \mathcal{T} \cdot \\ &\quad (\mathcal{V}_{\gamma d} - \mathcal{V}_{\gamma} - A \cdot \tilde{\mathcal{F}}_{\gamma}) \\ &\quad + \sum_i (\mathcal{P}_i - \hat{\mathcal{P}}_i)^2 / \rho_i \end{aligned} \quad (16)$$

It follows from (10), (11), and (15) that

$$\dot{V} \leq -(\mathcal{V}_{\gamma d} - \mathcal{V}_{\gamma} - A \cdot \tilde{\mathcal{F}}_{\gamma})^T \cdot \mathcal{K} \cdot (\mathcal{V}_{\gamma d} - \mathcal{V}_{\gamma} - A \cdot \tilde{\mathcal{F}}_{\gamma}) \quad (17)$$

It gives L_2 and L_{∞} stability with

$$(\mathcal{V}_{\gamma d} - \mathcal{V}_{\gamma} - A \cdot \tilde{\mathcal{F}}_{\gamma}) \in L_2 \cap L_{\infty} \quad (18)$$

Equ. (18) guarantees that a combination of velocity and filtered force $\mathcal{V}_{\gamma} - A \cdot \tilde{\mathcal{F}}_{\gamma}$ approached the reference $\mathcal{V}_{\gamma d}$ with L_2 and L_{∞} stability. Each parameter is updated within its lower and upper bounds independently through (14). But, there is no guarantee for parameters convergence.

3 Bilateral Teleoperation

Previous experiments have shown that the proposed adaptive motion/force control has excellent stability and motion/force tracking capability. In [10], conventional industrial robots perform very delicate operations using this controller. In this section, we apply it to teleoperation by designing suitable input signals $\mathcal{V}_{\gamma d}$ for both the master ($\gamma = h$) and the slave ($\gamma = e$).

(18) can be rewritten as

$$\rho_e \triangleq (\mathcal{V}_{ed} - \mathcal{V}_e - A \cdot \tilde{\mathcal{F}}_e) \in L_2 \cap L_{\infty} \quad (19)$$

$$\rho_h \triangleq (\mathcal{V}_{hd} - \mathcal{V}_h - A \cdot \tilde{\mathcal{F}}_h) \in L_2 \cap L_{\infty} \quad (20)$$

The teleoperation controller is written as

$$\begin{aligned} \mathcal{V}_{ed} &= \kappa_p \cdot \tilde{\mathcal{V}}_h + \lambda \cdot (\kappa_p \cdot \tilde{\mathcal{P}}_h - \delta \cdot \mathcal{P}_e) \\ &\quad - A \cdot \kappa_f \cdot \tilde{\mathcal{F}}_h \end{aligned} \quad (21)$$

$$\begin{aligned} \mathcal{V}_{hd} &= \frac{1}{\kappa_p} \cdot \left\{ \tilde{\mathcal{V}}_e + \lambda \cdot (\delta \cdot \tilde{\mathcal{P}}_e - \kappa_p \cdot \mathcal{P}_h) \right. \\ &\quad \left. - A \cdot [\tilde{\mathcal{F}}_e + (\kappa_f - \kappa_p) \cdot \tilde{\mathcal{F}}_h] \right\} \end{aligned} \quad (22)$$

where \mathcal{P}_h and \mathcal{P}_e denote the master and slave positions, respectively ($\mathcal{P}_h = \mathcal{V}_h$, $\mathcal{P}_e = \mathcal{V}_e$). κ_p and κ_f denote the motion scaling and the force scaling, respectively. δ is a binary selection function between position-force mode and rate-force mode, and is defined as

$$\delta = \begin{cases} 1 & \text{position/force mode} \\ 0 & \text{rate/force mode} \end{cases} \quad (23)$$

$\lambda > 0$ is a control parameter.

$\tilde{\mathcal{V}}_h$, $\tilde{\mathcal{V}}_e$, $\tilde{\mathcal{P}}_h$, and $\tilde{\mathcal{P}}_e$ are obtained by

$$\dot{\tilde{\mathcal{V}}}_h + C \cdot \tilde{\mathcal{V}}_h = C \cdot \mathcal{V}_h \quad (24)$$

$$\dot{\tilde{\mathcal{V}}}_e + C \cdot \tilde{\mathcal{V}}_e = C \cdot \mathcal{V}_e \quad (25)$$

$$\dot{\tilde{\mathcal{P}}}_h + C \cdot \tilde{\mathcal{P}}_h = C \cdot \mathcal{P}_h \quad (26)$$

$$\dot{\tilde{\mathcal{P}}}_e + C \cdot \tilde{\mathcal{P}}_e = C \cdot \mathcal{P}_e \quad (27)$$

Remark 1: The teleoperation design (21) and (22) makes $\tilde{\mathcal{V}}_{hd}$ and $\tilde{\mathcal{V}}_{ed}$ functions of \mathcal{V}_h , \mathcal{V}_e , \mathcal{F}_h , and \mathcal{F}_e , in terms of (11), (12), (24), and (25). Therefore, no acceleration measurement is required.

Substituting (21) and (22) into (19) and (20), and doing summation and subtraction yield

$$\begin{aligned}\rho_e - \kappa_p \cdot \rho_h &= \kappa_p \cdot \tilde{\mathcal{V}}_h - \tilde{\mathcal{V}}_e + \lambda \cdot [\kappa_p \cdot \tilde{\mathcal{P}}_h - \delta \cdot \tilde{\mathcal{P}}_e] \\ &\quad + \kappa_p \cdot \mathcal{V}_h - \mathcal{V}_e \\ &\quad + \lambda \cdot [\kappa_p \cdot \mathcal{P}_h - \delta \cdot \mathcal{P}_e]\end{aligned}\quad (28)$$

$$\begin{aligned}\rho_e + \kappa_p \cdot \rho_h &= \kappa_p \cdot (\tilde{\mathcal{V}}_h - \mathcal{V}_h) + \tilde{\mathcal{V}}_e - \mathcal{V}_e \\ &\quad + \lambda \cdot \kappa_p \cdot (\tilde{\mathcal{P}}_h - \mathcal{P}_h) + \delta \cdot \lambda \cdot (\tilde{\mathcal{P}}_e - \mathcal{P}_e) \\ &\quad - 2 \cdot A \cdot (\tilde{\mathcal{F}}_e + \kappa_f \cdot \tilde{\mathcal{F}}_h)\end{aligned}\quad (29)$$

A lemma is introduced as follows

Lemma 1: Suppose $\dot{x} + c \cdot x \in L_2 \cap L_\infty$, where c is a constant, it follows that $\dot{x} \in L_2 \cap L_\infty$ and $x \in L_2 \cap L_\infty$.

The proof is immediate by using $\int_0^t \dot{x} \cdot x dt \geq -\frac{1}{2} \cdot x(0)^2$.
Let

$$\mathcal{X} \triangleq \kappa_p \cdot \mathcal{V}_h - \mathcal{V}_e + \lambda \cdot [\kappa_p \cdot \mathcal{P}_h - \delta \cdot \mathcal{P}_e] \quad (30)$$

(28) can be rewritten as

$$\tilde{\mathcal{X}} + \mathcal{X} = \rho_e - \kappa_p \cdot \rho_h \quad (31)$$

where

$$\tilde{\mathcal{X}} + C \cdot \tilde{\mathcal{X}} = C \cdot \mathcal{X} \quad (32)$$

Substituting (32) into (31) and using Lemma 1 yield $\tilde{\mathcal{X}} \in L_2 \cap L_\infty$, $\tilde{\mathcal{X}} \in L_2 \cap L_\infty$, and further

$$\mathcal{X} \in L_2 \cap L_\infty \quad (33)$$

In the case of position-force control ($\delta = 1$), it follows from (30), (33), and Lemma 1 that

$$\rho_p \triangleq \kappa_p \cdot \mathcal{V}_h - \mathcal{V}_e \in L_2 \cap L_\infty \quad (34)$$

$$\kappa_p \cdot \mathcal{P}_h - \mathcal{P}_e \in L_2 \cap L_\infty \quad (35)$$

(34) and (35) guarantee L_2 stability for both velocity and position tracking.

In the case of rate-force control ($\delta = 0$), the slave velocity is controlled by the master position, while the master has the force feedback from the slave. It follows from (30) that

$$\rho_r \triangleq \kappa_p \cdot \mathcal{V}_h + \lambda \cdot \kappa_p \cdot \mathcal{P}_h - \mathcal{V}_e \in L_2 \cap L_\infty \quad (36)$$

The velocity of the slave \mathcal{V}_e tracks the position of the master \mathcal{P}_h with gain $\lambda \cdot \kappa_p$.

Premultiplying $(C^{-1} \cdot s + I_6)$ to both sides of (29) and using (12), (25), and (24) yield

$$\begin{aligned}& -(\mathcal{F}_e + \kappa_f \cdot \mathcal{F}_h) \\ &= \frac{1}{2} \cdot A^{-1} \{ C^{-1} \cdot [(s + \lambda) \cdot \kappa_p \cdot \mathcal{V}_h + (s + \delta \cdot \lambda) \cdot \mathcal{V}_e] \\ &\quad + (C^{-1} \cdot s + I_6) \cdot (\rho_e + \kappa_p \cdot \rho_h) \}\end{aligned}\quad (37)$$

where s denotes the Laplace derivative operator. In view of (34) and (36), (37) can be rewritten as

$$-(\mathcal{F}_e + \kappa_f \cdot \mathcal{F}_h) = A^{-1} \cdot C^{-1} \cdot (s + \lambda) \cdot \kappa_p \cdot \mathcal{V}_h + \frac{\rho}{2} \quad (38)$$

where

$$\begin{aligned}\rho &= A^{-1} \cdot [-\delta \cdot C^{-1} \cdot (s + \lambda) \cdot \rho_p \\ &\quad - (1 - \delta) \cdot C^{-1} \cdot s \cdot \rho_r \\ &\quad + (C^{-1} \cdot s + I_6) \cdot (\rho_s + \kappa_p \cdot \rho_m)]\end{aligned}$$

It follows that

$$-\mathcal{F}_h = \frac{\kappa_p}{\kappa_f} A^{-1} \cdot C^{-1} \cdot (s + \lambda) \cdot \mathcal{V}_h + \frac{1}{\kappa_f} \mathcal{F}_e + \frac{\rho}{2 \cdot \kappa_f} \quad (39)$$

Remark 2: This equation gives transparency of the whole teleoperation system. The term in the left hand side denotes the force from the operator toward the master. The first term in the right hand side indicates that the teleoperation system behaves as a free-floating mass plus a linear damper. The equivalent mass $(\kappa_p/\kappa_f)A^{-1}C^{-1}$ and damping $(\kappa_p/\kappa_f)A^{-1}C^{-1}\lambda$ parameters are completely specified by the control and scaling parameters, and not by the system parameters. The second term in the right hand side denotes the contribution of the operator force to the task execution. The last term in the right hand side is an error term containing derivatives of functions in L_2 . The results of bilateral teleoperation control in both position-force mode and rate-force mode can be summarized into the following theorem:

Theorem 1: For a bilateral teleoperated system in which both the master and the slave are subject to independent adaptive motion/force control and obey (19) and (20), applying the teleoperation controller design (21) and (22) results in:

a) asymptotic motion (velocity/position) tracking (34) and (35) under position-force mode and (36) under rate-force mode;

b) an overall teleoperation system equivalent to a free-floating mass plus a linear damper. The mass and the damping matrices are completely specified by the control and scaling parameters $(\kappa_p/\kappa_f)A^{-1}C^{-1}$ and $(\kappa_p/\kappa_f)A^{-1}C^{-1}\lambda$, respectively.

▽ ▽ ▽

4 Block Diagram Representation

A block diagram of 1-DOF teleoperation system with the control laws (11), (21), and (22) is illustrated in Fig. 5, where

$$C^m = \mathcal{K}^m + \frac{\mathcal{K}_I^m}{s} - (\hat{b}_h + \frac{\hat{k}_h}{s}) \quad (40)$$

$$G_b^m = (\hat{M}^m + \hat{m}_h) \cdot s + \mathcal{K}^m + \frac{\mathcal{K}_I^m}{s} \quad (41)$$

$$G_a^m = \frac{AC}{s+C} \cdot G_b^m \quad (42)$$

$$C^s = \mathcal{K}^s + \frac{\mathcal{K}_I^s}{s} - (\hat{b}_e + \frac{\hat{k}_e}{s}) \quad (43)$$

$$G_b^s = (\hat{M}^s + \hat{m}_e) \cdot s + \mathcal{K}^s + \frac{\mathcal{K}_I^s}{s} \quad (44)$$

$$G_a^s = \frac{AC}{s+C} \cdot G_b^s \quad (45)$$

$$C_1 = \frac{(s+\lambda)C}{s(s+C)} \cdot \kappa_p \cdot G_b^s \quad (46)$$

$$C_2 = \frac{1}{\kappa_p} \cdot G_a^m \quad (47)$$

$$C_3 = \kappa_f \cdot G_a^s \quad (48)$$

$$C_4 = \frac{(s+\delta\lambda)C}{s(s+C)} \cdot \frac{1}{\kappa_p} \cdot G_b^m \quad (49)$$

M^m and M^s denote the masses of the master and the slave, respectively. \mathcal{K}_I^m and \mathcal{K}^m denote the PD feedback gains for the master, while \mathcal{K}_I^s and \mathcal{K}^s denote the PD feedback gains for the slave.

Assume that the parameter uncertainties are completely compensated by parameter adaptation. By defining $\mathcal{F}^m = \mathcal{F}_h$, $\mathcal{V}^m = \mathcal{V}_h$, $\mathcal{F}^s = \mathcal{F}_e$, $\mathcal{V}^s = \mathcal{V}_e$, $\mathcal{F}^m = \mathcal{Z}_h \cdot \mathcal{V}^m$ and $\mathcal{F}^s = \mathcal{Z}_e \cdot \mathcal{V}^s$, it follows from Fig. 5 that

$$\begin{aligned} & \left(\kappa_p \cdot \frac{s+\lambda}{s} + \kappa_f \cdot \frac{AC}{s+C} \cdot \mathcal{Z}_h \right) \cdot \mathcal{V}^m \\ &= \left(\frac{(s+\delta\lambda)C}{s(s+C)} - \frac{AC}{s+C} \cdot \mathcal{Z}_e \right) \cdot \mathcal{V}^s \quad (50) \\ & \left(\frac{s+\delta\lambda}{s} + \frac{AC}{s+C} \cdot \mathcal{Z}_e \right) \cdot \mathcal{V}^s \\ &= \left(\kappa_p \cdot \frac{(s+\lambda)C}{s(s+C)} - \kappa_f \cdot \frac{AC}{s+C} \cdot \mathcal{Z}_h \right) \cdot \mathcal{V}^m \quad (51) \end{aligned}$$

Changing the sides of (51) and doing summation with (50) yield

$$(s+\delta \cdot \lambda) \cdot \mathcal{V}^s = (s+\lambda) \cdot \kappa_p \mathcal{V}^m \quad (52)$$

This equation is consistent with (34)-(36).

Meanwhile, multiplying (50) by (51) results in

$$-\mathcal{Z}_h = \frac{\kappa_p}{\kappa_f} \cdot \frac{s+\lambda}{A \cdot C} + \frac{\kappa_p}{\kappa_f} \cdot \frac{s+\lambda}{s+\delta \cdot \lambda} \cdot \mathcal{Z}_e \quad (53)$$

This equation is consistent with (39). $-\mathcal{Z}_h = -\mathcal{F}^m/\mathcal{V}^m$ denotes the impedance of the teleoperation system viewed from the operator site. The first term in the right hand side indicates that the teleoperation system behaves as a mass $\frac{\kappa_p}{\kappa_f} \cdot \frac{1}{A \cdot C}$ plus a damper $\frac{\kappa_p}{\kappa_f} \cdot \frac{\lambda}{A \cdot C}$, while

the second term in the right hand side represents the environment impedance reflected to the operator site. When in position-force mode, where $\delta = 1$, the second term in the right hand side becomes $(\kappa_p/\kappa_f) \cdot \mathcal{Z}_e$, i.e. the impedance of the environment reflected to the master through motion/force scaling. When in rate-force mode, where $\delta = 0$, it becomes $\frac{\kappa_p}{\kappa_f} \cdot \frac{s+\lambda}{s} \cdot \mathcal{Z}_e$, a special impedance in rate-force mode. Transparency in rate-force mode is still maintained for high frequencies, but not for low frequencies. The switch-off frequency is $\lambda/2\pi$. The transparency error in both position-force and rate-force modes is completely characterized by the first term in the right hand side, which is independent of the control modes used.

The structure of the block diagram is similar to Lawrence's four-channel structure [6]. However, the principle for designing these communication channels is different. The communication channels C_1 to C_4 in Lawrence's approach perform inverse dynamic control. C_1 to C_4 are designed to cancel the dynamics of the master and slave robots so as to achieve a perfectly transparent block. However, inverse dynamic control behaves as open loop control which is very sensitive to uncertainties. Therefore, a small time delay and any dynamic uncertainty, such as joint friction, may deteriorate system performance and even cause instability. In the proposed approach, the master together with the operator, and the slave together with the environment, are treated as two separate blocks. Each block is subject to independent adaptive motion/force control. Therefore, the uncertainties in each block are well compensated by strong feedback control together with parameter adaptation. Compared to Fig. 2 in [6], there are two additional local force feedback loops in Fig. 5 formed by $\frac{\kappa_f}{\kappa_p} \cdot G_a^m$ and G_a^s , respectively, to enhance force control ability. The communication channels only perform natural communication tasks which transform the motion/force information from the master toward the slave and from the slave toward the master. Therefore, it is robust against uncertainties including time delay. This feature produces excellent motion (position/velocity) tracking and very good force tracking. The force tracking accuracy can be further improved by using a large force scaling κ_f . This type of motion/force tracking is novel and is not presented in previous stability guaranteed designs, such as [4].

5 Experiments

The experimental set-up consists of an one-axis master and an one-axis slave driven by MAXON Motors RE 035-071 with 4,000 pulse encoders. A planetary gear-head with 10:1 ratio and a harmonic drive with 50:1

ratio are put on the master site and on the slave site, respectively, to increase torques. Two force sensors UFS 3012A25 U560 by JR³ Inc. are used at the end-effectors of both the master and the slave. The distances between the centers of force sensors to the motor driving axes are 65mm for the master and 132mm for the slave, respectively. A handle for the operator is mounted on the force sensor of the master. An aluminum bar of 25mm diameter is fixed to the common base of the master/slave robots. Soft tissues, e.g. human hand, are put between the aluminum bar and the slave to simulate a soft contact environment. The friction forces reflected at the end-effectors of the master and slave robots are of the order of 0.4N and 6.0N, respectively. The feedback gains in (11) are set as $\mathcal{K} = 80.0$ for the master and $\mathcal{K} = 800.0$ for the slave. The control system is running with two sampling frequencies on a SPARC 1E VME board by FORCE COMPUTERS Inc. using the Vx-Works operating system. The high sampling frequency of 500Hz is used to calculate (11), (21), and (22), while the low sampling frequency of 100Hz is used to calculate (12), (14), and (24)-(27). Some experimental results are illustrated from Fig. 1 to Fig. 4. In these figures, solid lines represent the scaled motion/forces of the master and dashed lines represent the exact motion/forces of the slave.

Figs. 1 and 2 illustrate experimental results on position tracking and force tracking, respectively, under position-force teleoperation. The system starts with free motion and makes contact with the environment just after $t = 6.2s$. Scaling parameters are $\kappa_p = 1.0$ and $\kappa_f = 2.0$. Control parameters are $A = 0.002$, $C = 50.0$, and $\lambda = 1.0$. The tracking results for both position and force are very good. The large force error in free motion results from the fact that the teleoperation system behaves as a mass plus a damper.

Figs. 3 and 4 illustrate experimental results on velocity tracking and force tracking, respectively, under rate-force teleoperation. Scaling parameters are $\kappa_p = 1.0$, $\lambda = 10.0$, $\kappa_f = 2.0$ and control parameters are $A = 0.002$, $C = 50.0$. The tracking performance for both velocity and force is also very good. Fig. 3 shows the velocity tracking error, Note that the solid line denotes a combination of velocity and position of the master, i.e. $\mathcal{V}_h + \lambda\mathcal{P}_h$. The noise spikes in Fig. 3 result from the velocity recording which is derived from encoder reading. Since 500Hz sampling frequency is used for feedback control, these noise spikes are actually 500 times encoder resolution. The system feels very stable.

6 Conclusion

In this paper, a novel controller design has been pro-

posed for bilateral teleoperation under both position and rate control modes with arbitrary motion/force scaling. No acceleration measurement is required. Compared to previous teleoperation controllers, this approach possesses three novel features: First, it is always L_2 and L_∞ stability guaranteed so as to provide a solid basis for achieving good transparency. The overall master/slave teleoperated system is equivalent to a free-floating mass plus a linear damper specified by the control and scaling parameters, which allows asymptotic motion tracking and force tracking. Second, system uncertainties are well compensated by applying independent parameter adaptation and strong feedback control. Third, the control design assumes nonlinear dynamic models of the robots incorporating the human operator and the environment. Benefitting from using the *virtual decomposition* approach, only the dynamics of rigid links and the dynamics of joints are required to construct the dynamics of the master/slave robots. Experiments have shown excellent results in motion tracking and very good results in force tracking.

References

- [1] T. B. Sheridan, "Telerobotics," *Automatica*, vol.25, no.4, pp.487-507, 1989.
- [2] B. Hannaford, "A design framework for teleoperators with kinesthetic feedback," *IEEE Trans. Robotics and Automation*, vol.5, no.4, pp.426-434, 1989.
- [3] K. Kosuge, J. Ishikawa, K. Furuta, and M. Sakai, "Control of single-master multi-slave manipulator system using VIM," *Proc. 1990 IEEE Int. Conf. Robotics and Automation*, pp.1172-1177, 1990.
- [4] R. J. Anderson and M. W. Spong, "Bilateral control of teleoperators with time delay," *IEEE Trans. Automatic Control*, vol.34, no.5, pp.494-501, 1989.
- [5] R. J. Anderson and M. W. Spong, "Asymptotic stability for force reflecting teleoperators with time delay," *Int. J. Robotics Research*, vol.11, no.2, pp.135-149, 1992.
- [6] D. A. Lawrence, "Stability and transparency in bilateral teleoperation," *IEEE Trans. Robotics and Automation*, vol.9, no.5, pp.624-637, 1993.
- [7] Y. Yokokohji and T. Yoshikawa, "Bilateral control of master-slave manipulators for ideal kinesthetic coupling-formulation and experiment," *IEEE Trans. Robotics and Automation*, vol.10, no.5, pp.605-620, 1994.
- [8] J. E. Colgate, "Robust impedance shaping telemanipulation," *IEEE Trans. Robotics and Automation*, vol.9, no.4, pp.374-384, 1993.
- [9] W. H. Zhu, Y. G. Xi, Z. J. Zhang, Z. Bien, and J. De Schutter, "Virtual decomposition based control for generalized high dimensional robotic systems with complicated structure," *IEEE Trans. Robotics and Automation*, vol.13, no.3, pp.411-436, 1997.

- [10] W. H. Zhu and J. De Schutter, "Experiment with two industrial robot manipulators rigidly holding an egg," *Proc. 1998 IEEE Int. Conf. Robotics and Automation*, pp.1534-1539, Leuven, Belgium, 1998.

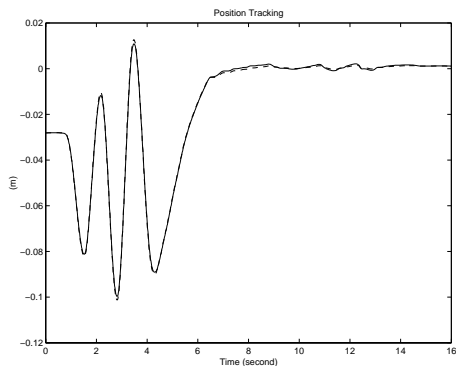


Fig. 1 Position tracking under position/force control

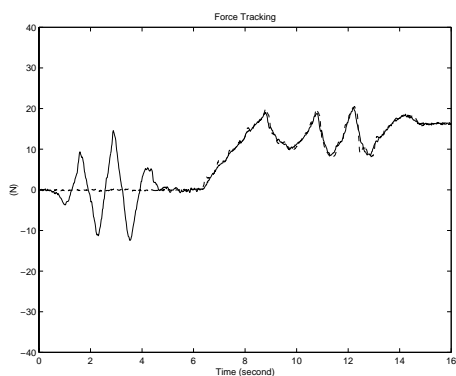


Fig. 2 Force tracking under position/force control

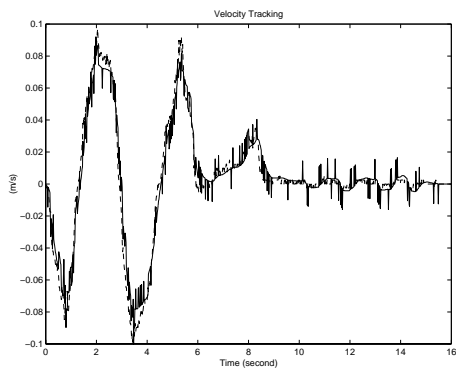


Fig. 3 Velocity tracking under position/force control

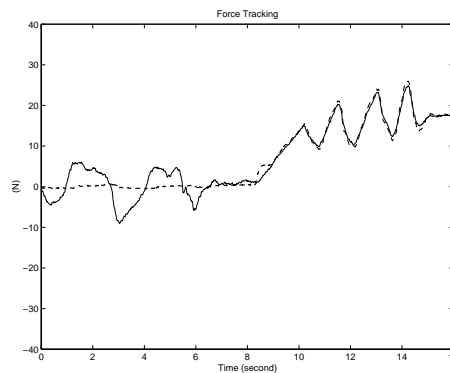


Fig. 4 Force tracking under position/force control

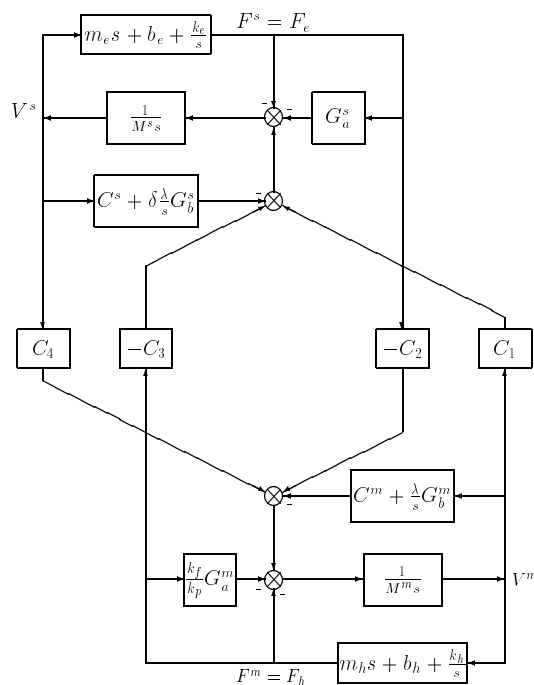


Fig. 5 Block diagram of an 1-DOF teleoperation system